applied sciences

MDPI

Article

Aluminium Assisted Nickel Alloying in Submerged Arc Welding of Carbon Steel: Application of Unconstrained Metal Powders

Theresa Coetsee * and Frederik De Bruin

Department of Materials Science and Metallurgical Engineering, University of Pretoria, Pretoria 0002, South Africa; fjdb.1953@gmail.com

* Correspondence: theresa.coetsee@up.ac.za

Abstract: Nickel alloying of carbon steel is used to enhance steel strength and toughness. Nickel alloying of the weld metal via solid weld wire presents several difficulties as highlighted previously, such as work hardening of the solid weld wire in manufacturing and feeding through the SAW wire feeding mechanism, and expensive and time consuming manufacturing of multiple weld wire formulations. The application of nickel and aluminium powders in unconstrained format, meaning not as fluxed cored wire or as metal cored wire, is used to simplify weld metal alloying. Al powder is used to control the oxygen potential at the weld pool-molten flux interface. The results presented here show that the addition of Al powder to the weld metal enhances Ni yield to the weld metal, at 85%, compared to pre-alloyed powder Ni yields of 57–78% as applied in previous work. Carbon steel was alloyed to 6.9% Ni and 3.7% Al. Thermodynamic analysis is applied to elucidate the chemical interaction between Ni and Al, and its effects on Ni yield in the weld pool. Overall process productivity gains stem from weld metal alloying from unconstrained metal powders because the expensive and time consuming step of manufacturing alloyed wire and alloyed powder is eliminated.

Keywords: pyrometallurgy; powder; nickel; oxygen control; aluminium; welding

Citation: Coetsee, T.; De Bruin, F. Aluminium Assisted Nickel Alloying in Submerged Arc Welding of Carbon Steel: Application of Unconstrained Metal Powders. *Appl. Sci.* **2022**, *12*, 5392. https://doi.org/10.3390/app12115392

Academic Editor: Anming Hu

Received: 23 April 2022
Accepted: 24 May 2022
Published: 26 May 2022

1. Introduction

Submerged Arc Welding (SAW) is applied in heavy engineering industries to join thick steel plates at high productivity rates, for example in the building of large seafaring ships, the construction of large offshore structures, and the construction of pressure vessels [1]. The SAW process is an electrical arc-based process in which chemical and electrical parameters are combined in the arc cavity to form an arc between the weld wire tip and the steel base plate. The arc cavity is formed by a layer of raw unmelted flux covering a layer of molten flux (slag), which in turn covers the arc to form the arc cavity. The arc cavity encapsulates the arc plasma, weld wire tip, and gasses emanating from the arc. Weld wire and flux are continuously fed through the welding head arrangement as it moves along the weld. As the weld wire is melted, the molten weld wire metal droplets are transferred from the weld wire into the weld pool. In addition to melting of the weld wire and arc formation, complex physical and chemical interactions of heat and mass transfer occur in the arc cavity [1]. Chemical reactions proceed in the trailing molten weld pool of molten steel and its covering slag, until the steel is solidified as weld metal [2,3]. Flux applied in the SAW process is made from a combination of oxides and fluorides, with the fluoride usually added as CaF_2. It is generally accepted from empirically determined measurements that the flux composition basicity index, the BI as expressed in Equation (1), should be larger than 1.5 in value to limit the weld metal hydrogen and weld metal total oxygen content (ppm O) to acceptable levels [4,5].

$$\mathrm{BI} = \frac{\%CaF_2 + \%CaO + \%MgO + \%BaO + \%SrO + \%Na_2O + \%K_2O + \%Li_2O + 0.5(\%MnO + \%FeO)}{\%SiO_2 + 0.5(\%Al_2O_3 + \%TiO_2 + \%ZrO_2)} \quad (1)$$

It has been confirmed experimentally that the stability of oxides in the arc plasma is not exactly the same as the expected thermodynamic stability of oxides. Welding tests were made under an argon gas atmosphere for different binary oxide-CaF_2 flux mixtures to show that the arc plasma stability sequence of oxides ranges from most stable to least stable as follows: CaO, K_2O, Na_2O and TiO_2, Al_2O_3, MgO, SiO_2, and MnO [6]. Thus, by increasing the flux CaF_2 content, the proportion of low stability oxides in the flux, and thus also in the molten flux (slag), is effectively diluted to ensure lower ppm O in the weld metal.

The importance of total weld metal oxygen content in setting the carbon steel weld metal materials properties was illustrated from weld metal impact toughness test weld metal samples of different ppm O. It was shown that high weld metal impact toughness is maintained if the total oxygen content is maintained within the band of 200 ppm O to 500 ppm [7]. Therefore, it is important to control the carbon steel weld metal total oxygen content within this ppm O range. In addition to the formulation of fluxes for oxygen and hydrogen control, the flux chemistry is formulated to achieve targeted element transfer levels from the slag to the weld metal [3,8–11]. Because nickel has a low affinity for oxygen, it is typically added to the weld pool from the alloyed weld wire. Nickel is often alloyed in the weld wire with chromium as stainless steel weld wires, and the weld wire chemistry is usually over matched to the base plate composition. Therefore, the fluxes used in SAW of chromium and/or nickel containing steel are neutral or non-alloyed [12]. If any metallic powders of chromium, nickel, molybdenum, or niobium are added into the flux formulation, this is only done to compensate for element loss across the arc [13]. Manufacturing of weld wires of specific compositions is expensive and time consuming and cannot closely match all desired alloy compositions. Therefore, the use of weld wire to alloy the weld metal with nickel is restricted to a limited number of weld wire formulations. Matched alloying of the weld metal may be better accomplished if the metal powder is applied to the welding process to achieve the aim weld metal composition [14,15]. Furthermore, efforts are made to develop flux cored wire for weld metal nickel alloying due to work hardening of the solid weld wire in manufacturing and in feeding the weld wire through the SAW wire feeding mechanism [16]. In this reported study two flux formulations of different basicity were tested under the same welding conditions, at BI of 1.4 and 2.8. Flux basicity affected the deposition rate and weld metal oxygen content, however, insignificant differences were reported on Ni yield from the flux cored wire to the weld metal, despite high weld metal ppm O values of 628 to 835 ppm O.

Similarly, Ni-containing pre-alloyed powders were applied in SAW to better control the required chemistry of coating applications via SAW [14]. The claimed benefits of using pre-alloyed powders for alloying in cladding, compared to alloying via the weld wire, are that weld metal dilution from the iron contained in the weld wire and dilution from the substrate steel are limited because the weld pool is cooled due to the melting of the added powders. Overall deposition productivity is also improved due to the application of metal powders. However, conversion of the reported analyses values to Ni yield values confirms that the Ni yield is less than 100%. Nickel yield values ranged from 57 to 78% from iron based alloy powders containing 27–29% Cr, 5–8% Ni, and 2–4% Mo. These nickel yield values appear to be much lower than the typical values of 100% nickel yield reported when solid weld wire is used in SAW [12,17].

In comparison, in conventional SAW with solid weld wire, some nickel and chromium loss values were reported as influenced by slag chemistry, although the base metal alloying element values were low: 0.3% Ni loss and 0.3% Cr loss from the welding base plate containing 1.65% Ni and 0.76% Cr when solid weld wire containing 0% Ni and 1.25% Cr was used. These values represent 81% Ni yield and 61% Cr yield in the presence of a highly oxidising flux of 40% SiO_2-MnO-CaO [18]. Although comparative welding tests with more oxidising flux (40% SiO_2-FeO-CaO) showed smaller element loss values for Ni and Cr,

and welding with a highly reducing basic flux (40% SiO_2-MnO-CaF_2) showed the lowest element loss values for Ni and Cr. Therefore, even when solid wire alloying is applied in SAW, the extent of the de-oxidiser effect of Cr on Ni yield, and its importance, are not clear.

Nickel is used as an alloying element in low-alloy steels and as an austenite stabiliser in stainless steels to counter the ferrite stabiliser effect of chromium. Nickel is added at levels up to 10% in aluminium killed cryogenic steels. Nickel may be used in combination with copper or cobalt as precipitation hardening agents [13]. Although aluminium is traditionally not added in large quantities in steel, the more recent development of low density/high-entropy steels and low density stainless steels requires high quantities of aluminium in the steel [19,20]. Therefore, the application of combinations of alloying elements with aluminium in SAW is an important contribution to expanding the application of SAW to these newer steel grades.

Addition of Fe powders in SAW is used to increase welding productivity in cladding applications and in weld joining of metal plates [15,21,22]. Significant productivity gains were achieved in the form of increased metal deposition rates, when iron metal powder was added in SAW [15,21,22]. This is possible because only 20% of the arc energy is used to melt the weld wire in conventional SAW which uses only solid weld wire [15]. A 50% increase in metal deposition rate to 10.4 kg/h was demonstrated when iron metal powder was added in SAW with input parameters of 500 A, 31 V and 60 cm/min travel speed in a two weld wire set-up, compared to 6.3 kg/h deposition rate achieved in the absence of iron metal powder addition, in the same SAW set-up with the same welding parameters used [22].

Limited published studies are available on the application of unconstrained (not fluxed cored wire or metal cored wire) metal powders for alloying purposes in SAW. In particular, the behaviour of nickel when used as an alloying powder is not clear since the percentage yield appears to be much lower than the 100% yield typically reported for solid weld wire alloying [12,17]. The objective of this study is to demonstrate the application of unconstrained nickel and aluminium powders in SAW to alloy the weld metal and control the weld metal oxygen content. Thermodynamic analysis is applied to elucidate the chemical interaction between Ni and Al and its effects on Ni yield from the unconstrained metal powder to the weld pool. Application of weld metal alloying from unconstrained metal powders will yield productivity gains in weld metal deposition rate and in eliminating the expensive time consuming step of manufacturing alloyed wire and alloyed powder because metal powders can be used directly in the unconstrained format [14,15,21,22].

2. Materials and Methods

The initial SAW experiment was conducted in the absence of metal powder additions to establish a base case (BC) as reference. Then, for the same welding conditions of welding heat input and using the same weld wire, metal powders (Al and Ni) were added to investigate the chemical interaction of nickel with aluminium. The latter is added to control the partial oxygen pressure at the weld pool-molten slag interface to control the weld pool oxygen content.

Bead-on-plate welding test runs were made onto steel plates of 350 mm length, 12 mm plate thickness, and 300 mm plate width. Weld heat input was 2.0 kJ/mm (500 A, 28 V, 42 cm/min) welded DCEP (direct current electrode positive) with 3.2 mm diameter wire. Commonly used structural steel of grade (S355J2+N) as specified by EN 10025-2 was used as base plate material. The weld wire major element levels are from the supplier's specification sheet as supplied by Afrox Ltd., Johannesburg, South Africa. The base plate steel was analysed by optical emission spectroscopy (OES) after surface preparation consisting of surface levelling. The oxygen content in the base plate and weld wire was analysed by the combustion method. Table 1 provides the complete weld wire and base plate analyses.

Table 1. Base plate and weld wire compositions (mass%).

	%C	%Si	%Mn	%O	%Al	%P	%S	%Ti	%Cu	%Cr	Balance
Plate	0.120	0.155	1.340	0.0007	0.067	0.019	0.007	0.005	0.030	0.160	Fe
Wire	0.110	0.137	0.990	0.0003	0.000	0.009	0.023	0.000	0.140	0.000	Fe

The welded plate was sectioned at the middle position of the weld run to remove cross section samples. A band saw was used to make sample cuts. Individual volume samples were cut of the whole weld bead from each cross section sample by using a manual saw, following surface preparation and 2% Nital solution etching to reveal the weld metal bead boundary in the base plate. One volume sample was analysed for major element analyses by inductively coupled plasma optical emission spectrocopy (ICP-OES). The second volume sample was used for total oxygen and carbon analysis by the combustion method. A third weld metal cross section sample was analysed by SEM (scanning electron microscope) following polishing to a mirror finish and etching with 2% Nital solution to reveal the weld metal boundary in the base plate. The SEM equipment consisted of a Zeiss (Oberkochen, Germany) crossbeam 540 FEG (Field emission gun) SEM with EDS (energy dispersive spectrometer) operated at 20 kV.

The flux selected for the welding tests is a commercial agglomerated flux of composition in Table 2. The main consideration in the selection of this flux, following initial testing of different fluxes, is its thermodynamic stability in the presence of aluminium metal [23]. This flux is classified as an aluminate basic flux (Basicity Index (BI) = 1.4) and its chemistry and mineralogy were extensively investigated previously [23]. This flux is agglomerated and has a 0.2–1.6 mm agglomerate particle size. Metal powders of pure Al (99.7% Al and 1 mm) supplied by Sigma-Aldrich, and pure Ni (99.5% Ni and 0.25 mm) supplied by GoodFellow were used.

Table 2. Flux bulk chemical composition (mass%).

MnO	CaO	SiO_2	Al_2O_3	CaF_2	MgO	FeO	TiO_2	Na_2O	K_2O
6.8	0.1	19.6	24.9	17.9	22.2	2.4	1.0	1.6	0.2

3. Results

3.1. Chemical Analyses

The weld metal compositions for the two scenarios, without metal powder addition (BC) and with metal powder addition (MP6), are summarised in Table 3. The SEM micrograph in Figure 1 and EDS analyses in Table 4 confirm the alloying of the weld metal with Ni and Al. The area selected for EDS analyses as shown in Figure 1 is positioned at the geometric centre of the weld metal cross section.

Table 3. Weld metal compositions (mass%).

	%C	%Si	%Mn	%O	%Al	%P	%S	%Ni	%Cr
Base Case	0.110	0.260	1.300	0.0499	0.032	0.022	0.011	0.005	0.110
MP6	0.111	0.390	1.653	0.0247	3.737	0.026	0.040	6.956	0.173

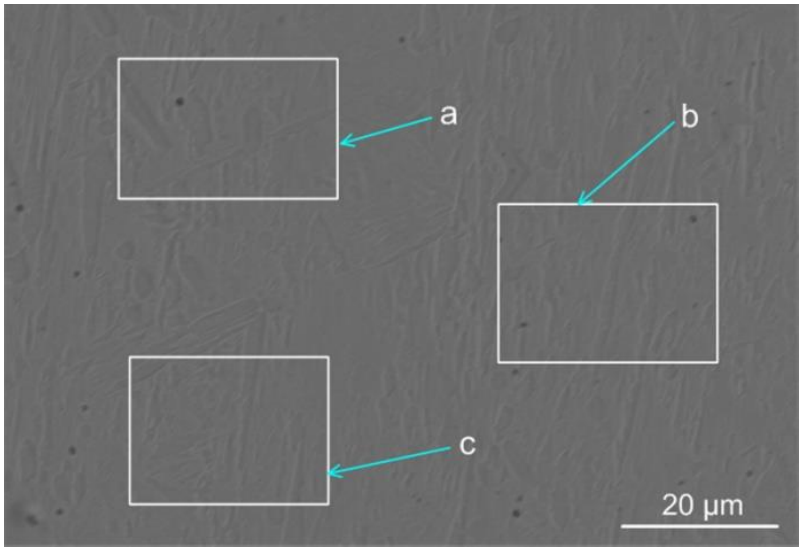

Figure 1. SEM micrograph of weld metal with analysed areas marked. (See Table 4 for the analyses of the marked phase areas: a–c) (×3000).

Table 4. SEM-EDS analyses of marked areas in the weld metal as indicated in Figure 1 (mass%).

	%Si	%Mn	%Al	%Ni	%Fe
a	0.83	1.37	2.40	7.29	87.8
b	0.80	1.70	2.60	7.21	87.7
c	0.80	1.60	2.50	7.30	87.8

The slight increase in silicon and manganese content of the MP6 weld metal confirms that some aluminothermic reduction of SiO_2 and MnO from the flux occurred via the reactions displayed in Equations (2) and (3). The ppm O is also significantly lowered from 499 ppm O to 247 ppm O due to the de-oxidiser effect of aluminium at the weld pool-slag interface [24–28].

Therefore, the MnO and SiO_2 in the slag were reduced by aluminium powder via reactions (2) and (3) as shown below. The FeO in the slag formed from excess oxygen transferred from the arc cavity, is also reduced by alumium powder via reaction (4) to control the oxygen potential at the weld pool-slag interface [24–28].

$$3(SiO_2) + 4(Al) = 3(Si) + 2(Al_2O_3) \quad \Delta H^{\circ}_{2000^{\circ}C} = -82.1 kJ/mol\ Al \quad (2)$$

$$3(MnO) + 2(Al) = 3(Mn) + (Al_2O_3) \quad \Delta H^{\circ}_{2000^{\circ}C} = -248.4\ kJ/mol\ Al \quad (3)$$

$$3(FeO) + 2(Al) = 3(Fe) + (Al_2O_3) \quad \Delta H^{\circ}_{2000^{\circ}C} = -416.5\ kJ/mol\ Al \quad (4)$$

( ): liquid.

The increased percentage of silicon and manganese in the MP6 weld metal, as compared to the base case (BC) weld metal, confirms that sufficient contact time was established between Al powder and flux to enable reactions (2) and (3) to forward to a significant extent. The Al_2O_3 products formed from reactions (2) and (3) were absorbed into the molten flux since these reactions occurred at the molten flux-weld pool interface [24–28].

3.2. Mass Balance

The following mass measurements and mass balance calculations were made to quantify the yield of Ni and Al to the weld metal. This calculation procedure is the same procedure applied previously [26–28]. The steel plate mass was recorded before and after welding, and the mass difference then quantifies the mass of weld wire and metal powder added to the weld metal. A cross section cut of the weld metal was polished to a mirror

finish and then etched with 2% Nital solution to reveal the weld metal boundary in the base plate. The etched cross section was used to measure the weld metal areas above and below the base plate top surface level from stereoscope images of the weld metal cross section, using the stereoscope software. The areas are marked in Figure 2 for both weld metal cross section images: the area between line A and line B is the proportional area above the base plate top surface level. This is the proportion of the weld metal contributed by the weld wire and metal powder, namely Area 1. The proportional area between line B and line C is the proportion of the weld metal area contributed by the melting of the base plate, namely Area 2. Here, this area proportion is defined as the dilution ratio as previously reported and named ($\%DR_{(wire+MP)}$) in the following expressions [26–28].

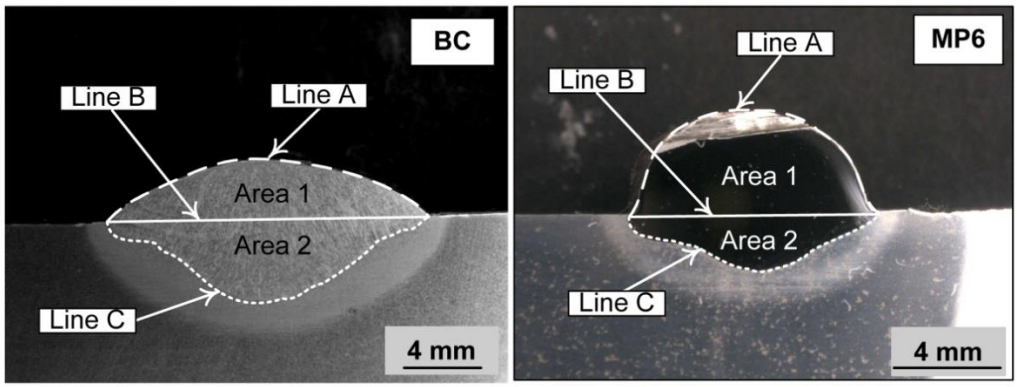

Figure 2. Weld metal cross section micrographs via stereoscope.

The mass Al and Ni added to the weld metal were calculated from Equations (5)–(7). The weld metal composition in Table 3 is used as input to Equation (7). The expressions in Equations (5)–(7) illustrate the calculation sequence for aluminium. Similarly, the calculation for nickel is made by using the %Ni in the weld metal from Table 3 as input to Equation (7).

$$\%DR_{(wire+MP)} = \left(\frac{A_{(wire+MP)}}{A_{(wire+MP)} + A_{BP}}\right) \times 100 = \left(\frac{Area1}{Area1+Area2}\right) \times 100 \quad (5)$$

$$m_{WM} = (m_{wire} + m_{MP}) \times \left(\frac{100}{\%DR_{(wire+MP)}}\right) \quad (6)$$

$$(\text{gram Al to WM}) = (m_{WM}) \times \left(\frac{\%Al_{WM}}{100}\right) \quad (7)$$

WM = weld metal; MP = metal powder; BP = base plate; Wire = weld wire; m = mass (gram); A = area (mm^2).

Once the grams of Al and Ni added to the weld metal are calculated from Equations (5)–(7), the percentage yield of each element to the weld metal is calculated from the initial input mass of 7 grams of Al, and 7 grams of Ni. Table 5 summarises the numbers applied in Equations (5)–(7), and the calculation results from Equation (7). The resultant percentage yield numbers for Ni and Al are 85% and 45%, respectively.

Table 5. Mass balance numbers for percentage yield calculation.

	Al (g)	Ni (g)	Powder (g)	Wire (g)	BasePlate (g)	Weld Metal (g)	$\%DR_{(wire+MP)}$	%Al Yield	%Ni Yield
Base Case	0	0	0	33.8	33.8	67.6	50	0	0
MP6	3.2	6.0	9.2	50.7	26.4	86.3	69	45	85

The exothermic reaction heat contributions from Equations (2) and (3) are calculated by first quantifying the mass of Mn and Si added to the weld metal from these reactions by using Equation (8) as reported previously [26–28]. Equation (8) shows the calculation for the mass of Mn added from aluminothermic reduction, (M_{Mn}). The inputs to Equation (8) are the weld metal mass, (Mwm) and the dilution ratio value, ($\%DR_{(wire+MP)}$) from Table 5 for the base case, and the %Mn in the weld metal from Table 3. The square bracketed terms in Equation (8) represent the calculation of the BC weld metal nominal composition.

$$M_{Mn} = (M_{WM})\left(\frac{\%Mn_{WM}}{100} - \left[\frac{\%DR_{wire}}{100} \times \frac{\%Mn_{wire}}{100}\right] - \left[\left(1 - \frac{\%DR_{wire}}{100}\right) \times \frac{\%Mn_{BP}}{100}\right]\right) \quad (8)$$

M = mass (gram); M_{WM} = mass Mn (gram); $\%Mn_{WM}$ = %Mn in weld metal; %DR-wire = % of weld metal contributed by weld wire in the Base Case (BC); %Mnwire = %Mn in weld wire; $\%Mn_{BP}$ = %Mn in Base Plate (BP); WM = weld metal; BP = base plate; Wire = weld wire

The exothermic heat is calculated from the reaction enthalpy values displayed next to reactions (2) and (3). A simplified translation of the kJ values is made by using the heat capacity of steel (0.460 kJ/kg K) to calculate the expected increase in weld metal temperature due to reactions (2) and (3). The calculation results are summarised in Table 6. It is seen that although small quantities of SiO_2 and MnO were reduced into the weld metal via reactions (2) and (3), the exothermic effect of these reactions is significant in increasing the weld metal temperature by 53 °C. This exothermic heat may contribute to the melting of metal powders for incorporation into the weld pool.

Table 6. Exothermic heat added to the weld pool from reactions (2) and (3).

	SiO_2 (g)	MnO (g)	Al (g)	Reaction (2) (kJ)	Reaction (3) (kJ)	Reactions (2) & (3) (kJ)	Weld Metal ΔT (°C)
MP6	0.46	0.54	0.41	−0.83	−1.27	−2.1	53

Furthermore, the weld pool solidification time is an important aspect of oxygen content control of the weld pool. Increased weld pool cooling time provides more time for oxide inclusions to float from the weld pool to the molten slag-weld pool interface to be absorbed into the molten slag [29]. The weld pool cooling time, set by the difference between the weld pool liquidus and solidus temperature, may be different for differing weld pool chemistries. This effect is shown in Figure 3 for the two weld metal chemistries displayed in Table 3.

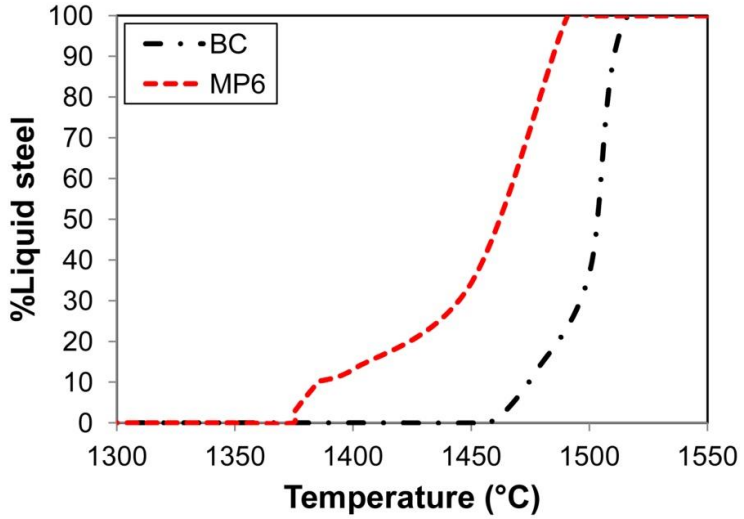

Figure 3. Solidification curves for BC and MP6 weld metal compositions as calculated in FactSage 7.3 [30].

The solidification curves in Figure 3 were calculated in FactSage 7.3 thermochemical software using the Equilib module and the FToxid and FSstel databases [30]. Figure 3 confirms that the solidus temperature of MP6 weld metal is significantly lower than the solidus temperature of the Base Case (BC) weld metal, and this aspect will contribute to a lower ppm O in the MP6 weld metal, compared to the BC weld metal, as is confirmed in Table 3.

4. Discussion

The results in Table 5 clearly show that the assumption of 100% Ni yield to the weld metal is not applicable in the application of unconstrained metal powders in SAW. The assumption of 100% Ni yield typically used in solid weld wire application in SAW is based on the low oxygen affinity of Ni for oxygen, indicating that Ni should not be oxidised from the weld pool to form NiO which ends up in the welding slag [12,17]. Comparison to literature reported values of Ni yield in the application of different Ni-alloying consumables illustrates that differences in Ni-yield are seen for different consumable configurations such as solid weld wire vs. alloyed metal powders.

For example, in the application of pre-alloyed powders in SAW the demonstrated application used iron based powder containing 27–29% Cr, 5–8% Ni, and 2–4% Mo [14]. Interestingly, the nickel yield from these pre-alloyed powders ranged from 59% to 74% when the "direct feeding" powder feed mode was applied [14]. This feeding mode consisted of magnetically attaching the pre-alloyed powder to the weld wire as a surface coating. In a comparative test, the same pre-alloyed powder feed material at the same feed rate, using one arcing weld wire only, was applied for two feeding modes, namely "direct feeding" described above vs. "forward feeding" of the powder onto the substrate steel plate, in advance of the welding head. The alloying element yields of Ni, Cr, and Mo to the weld metal were similar for the two feeding modes and within the following ranges: 57–59% Ni yield, 56–58% Cr yield, and 55–58% Mo yield from the pre-alloyed powder to the weld metal [14]. Here, in the presence of Al as a de-oxidiser, the Ni yield is higher than the yields from pre-alloyed powder application in SAW. In the following section a thermodynamic analysis is applied to elucidate the chemical interaction between Ni and Al, and its effects on Ni yield in the weld pool.

Several complex reactions take place in the arc cavity and may contribute to Ni loss in SAW. For example, some of the Ni is expected to vaporise, Ni may react with F_2(g) and/or CaF_2(g) to form NiF_2(g), and Ni may also oxidise to NiO. Thermodynamic calculations were applied to further investigate the relative likelihood of the possible reactions of NiF_2(g) formation, relative to similar reactions from different compounds contained in the flux, metal powders, and steel. Reactions of the type in Equations (9) and (10) were considered, and the standard Gibbs free energy graphs for these reactions are displayed in Figures 4 and 5. The standard Gibbs free energy values were calculated in FactSage 7.3 thermochemical software [30]. The temperature interval of 1600 °C to 2500 °C is used to illustrate the temperature band of the main reactions in SAW as identified in previous works, namely 2000 °C for slag-metal equilibrium reactions and 2500 °C at the arc plasma-weld pool interface [2,3,31].

$$[Ni] + [F_2] = [NiF_2] \quad (9)$$

$$(NiO) + [CaF_2] = [NiF_2] + \langle CaO \rangle \quad (10)$$

( ): liquid; [ ]: gas; < >: solid.

Chemical values applied as inputs to the Figure 4 calculations were 1 atm for each gas, namely metal vapour, F_2(g), and the product metal fluoride gas. Chemical values applied as inputs to the Figure 5 calculations were 1 atm CaF_2(g), unit activity for the molten metal oxides, 0.10 atm for the metal fluoride gas formed, and 0.01 activity for the CaO formed from reaction (10). According to the standard Gibbs free energy values displayed in Figure 4, the formation of NiF_2(g) is least likely among the metal vapour reactions with F_2(g). However, in comparison to the standard Gibbs free energy values in Figure 5, all

reactions of type (9) are more likely to occur than reactions of type (10). Therefore, the reaction of NiO with $CaF_2(g)$ is less likely than the reaction of Ni(g) with $F_2(g)$ for $NaF_2(g)$.

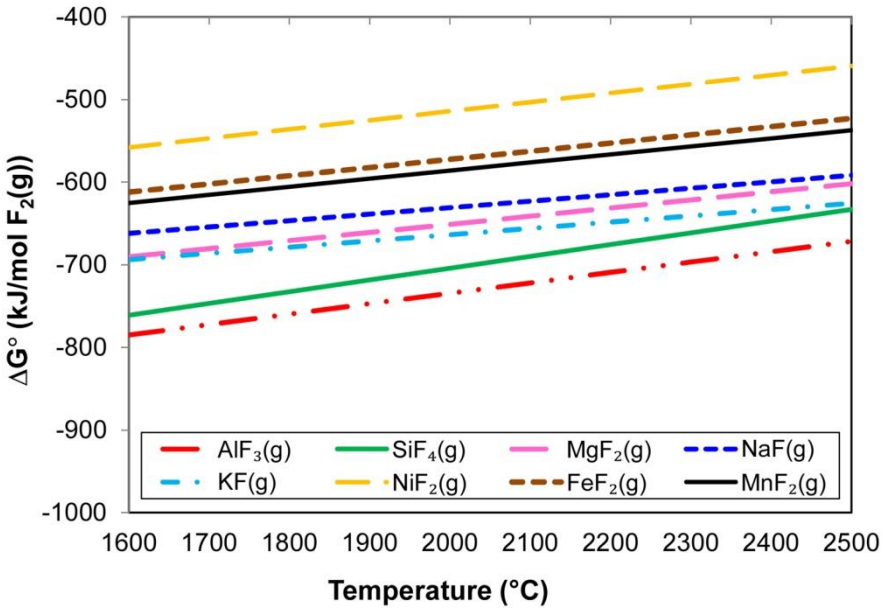

Figure 4. Standard Gibbs free energy for metal vapour and F_2 gas reactions as calculated in FactSage 7.3 [30].

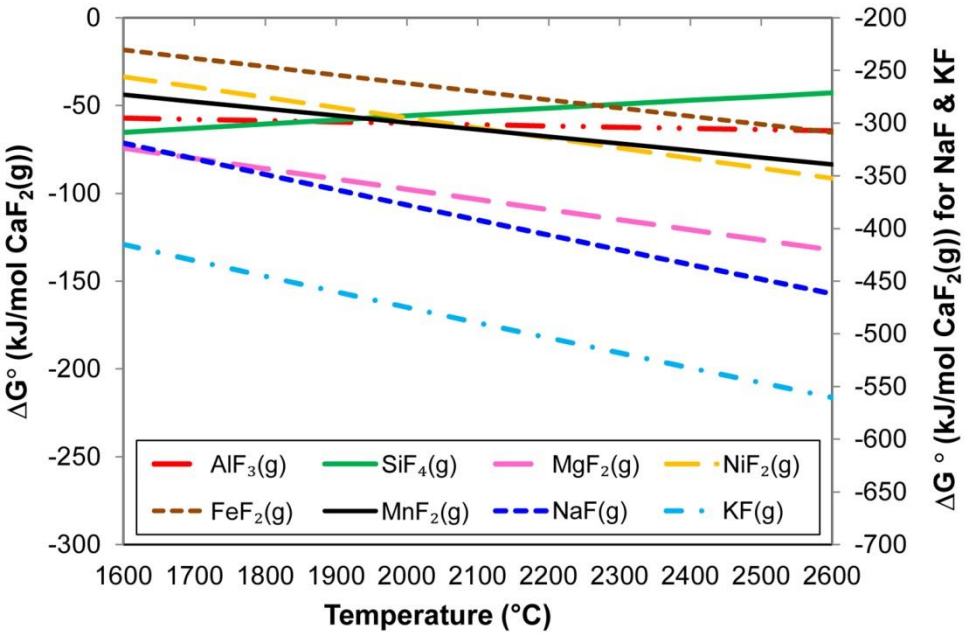

Figure 5. Standard Gibbs free energy for metal oxide and CaF_2 gas reactions as calculated in FactSage 7.3 [30].

Therefore, the likely reaction sequence for the application of aluminium and nickel powders in an unconstrained format in SAW is shown in Figure 6. Reaction steps A to E are as presented in previous works [6,31–34]. It was conclusively shown that an excessive quantity of oxygen is initially added to the molten weld wire droplets from the arc cavity gas phase, up to 2000–3000 ppm O [31,32]. The word "excessive" means that the ppm O in the weld pool exceeds the solubility limit of oxygen at the cooling weld pool temperature once the arc has passed and the weld pool cools to lower temperatures from the high arc plasma temperatures, typically 2000–2500 °C [2,3,33]. This initial excessive oxygen

quantity in the metal droplets is sourced from the decomposition of less stable oxides at the high temperatures prevailing in the arc plasma, and so flux chemistry is used to manage oxygen transfer to the weld metal from the arc plasma [6]. Based on the arc plasma stability hierarchy of oxides, MnO, SiO_2, MgO, and Al_2O_3 contained in the flux, as presented in Table 2, may all dissociate in the arc plasma to release oxygen in the arc cavity to adsorb onto the molten weld wire droplets, reactions A to C in Figure 6 [6].

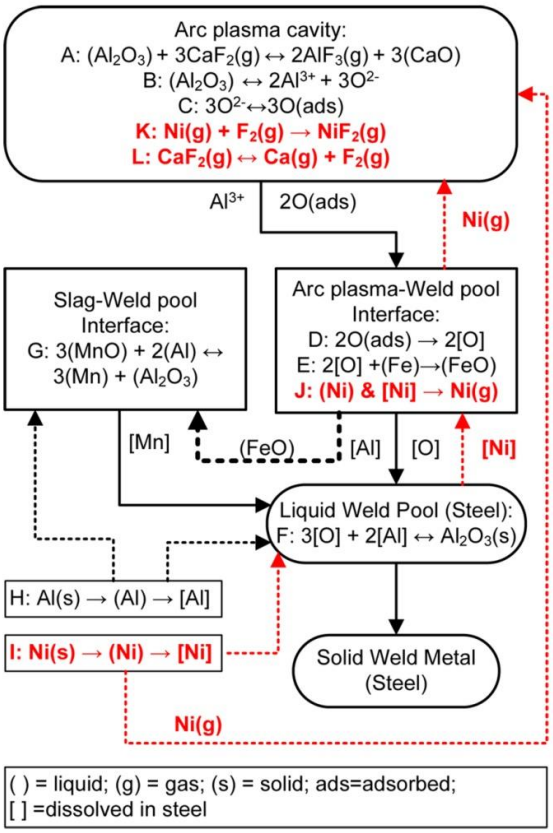

Figure 6. SAW reaction flow diagram with Al and Ni powder additions.

It is clear from previous work that the excessive quantity of oxygen transferred from the arc cavity reacts with the molten steel at the arc plasma-weld pool interface to form FeO, reaction E. This FeO is incorporated into the slag. The correlation of increased FeO in the molten flux with increased weld metal ppm O is well known [17,35–39]. The oxygen potential prevailing at the molten flux-weld pool interface, as presented by the quantity of FeO in the slag, is reduced in this work by adding Al powder. Similar to reaction G for the reduction of MnO from the molten flux, FeO is also reduced by aluminium, see reaction (4) in the text. These aluminium based reduction reactions, the reactions as displayed in Equations (2)–(4) in the text, are exothermic and therefore release chemical energy in the form of heat into the weld pool. This extra added heat can be used to melt and dissolve nickel powder into the weld pool.

The reduced oxygen potential at the molten flux-weld pool interface prevents oxidation of Ni powder to NiO, and so prevents loss of Ni to the slag. Instead, the Ni powder is melted and dissolved into the weld pool, see reaction I. Since there is an excess of Al added, some of the Al also dissolves into the weld pool, see reaction H. Based on the standard Gibbs free energy values displayed in Figures 4 and 5 it appears that Ni loss in SAW with metal powder alloying occurs due to Ni vaporisation and/or subsequent reaction of Ni vapour with Fluorine gas to form $NiF_2(g)$. This reaction sequence is marked in red text as reactions J, K, and L in Figure 6. Nickel can be vapourised at the arc plasma-weld pool interface from the weld pool and from the unconstrained Ni powder, before it is dissolved into the weld pool. The $F_2(g)$ formation from the dissociation of $CaF_2(g)$ in the arc plasma

appears possible since the Ca and F were analysed in the arc cavity gas phase when a CaF_2 based flux was used in SAW [1,34]. This reaction sequence may explain why Ni element transfer in SAW as reported in the literature is lower when Ni is alloyed in the form of pre-alloyed Cr containing powders. Cr or Al de-oxidisers added with Ni powder or pre-alloyed powder ensure that the Ni remains as Ni metal to vaporise easily in the arc cavity. In contrast, Ni contained in weld wire has less exposed surface area than metal powders, and therefore less Ni will be vaporised and/or oxidised from the weld wire during melting.

The results presented here confirm that the oxygen potential at the molten flux-weld pool interface is lowered by Al powder addition and this effect plays a role in the element transfer of Ni into the weld pool, without interfering with oxygen transfer from the plasma arc to the weld pool. The thermodynamic analysis shows that the likely chemical reaction of Ni loss is due to the reaction of Ni vapour with F_2(g) to form NaF_2(g) in the arc cavity. The chemical interaction between Ni and Al occurs indirectly via reduced oxygen potential at the molten flux-weld pool interface, which maintains Ni in the metallic form and prevents oxidation of Ni to NiO.

5. Conclusions

1. Nickel recovery to the weld metal is improved in unconstrained metal powder application, compared to the application of with pre-alloyed nickel containing powder as reported in previous work;
2. Carbon steel weld metal was alloyed with unconstrained metal powders to 6.9% Ni and 3.7% Al, representing 85% Ni yield and 45% Al yield to the weld metal.
3. The aluminium powder addition ensured sufficient control of the oxygen potential at the molten flux–weld pool interface without interfering with oxygen transfer from the arc plasma to the weld pool, resulting in 247 ppm O in MP6 vs. 499 ppm O when no metal powder was added;
4. Thermodynamic assessment of metal fluoride gas formation reactions indicates that NiF_2(g) is more likely to form from vaporised Ni, than from NiO formed from Ni oxidation.
5. The aluminothermic reduction of SiO_2 and MnO from the molten flux (slag) heats the weld pool by approximately 53 °C.
6. Application of unconstrained metal powders in SAW improves overall process productivity because it eliminates the expensive time consuming step of the manufacturing of alloyed wire and alloyed powder because unconstrained metal powders can be applied directly in the SAW process.

Author Contributions: F.D.B. conceptualised the work; F.D.B. and T.C. executed the experiments, interpreted the data, and prepared the manuscript. All authors have read and agreed to the published version of the manuscript.

Funding: This research was funded in part by the National Research Foundation of South Africa, grant number BRIC171211293679.

Data Availability Statement: The data sets presented in this study are available upon request to the corresponding author.

Conflicts of Interest: The authors declare no conflict of interest. The funders had no role in the design of the study; in the collection, analyses, or interpretation of data; in the writing of the manuscript, or in the decision to publish the results.

References

1. Sengupta, V.; Havrylov, D.; Mendex, P.F. Physical phenomena in the weld zone of submerged arc welding—A Review. *Weld. J.* **2019**, *98*, 283–313.
2. Chai, C.S.; Eagar, T.W. Slag-metal equilibrium during submerged arc welding. *Metall. Trans. B* **1981**, *12*, 539–547. [CrossRef]
3. Mitra, U.; Eagar, T.W. Slag-metal reactions during welding: Part I. Evaluation and reassessment of existing theories. *Metall. Trans. B* **1991**, *22*, 65–71. [CrossRef]

4. Eagar, T.W. Sources of weld metal oxygen contamination during submerged arc welding. *Weld. J.* **1978**, *57*, 76–80.
5. Tuliani, S.S.; Boniszewski, T.; Eaton, N.F. Notch toughness of commercial submerged arc weld metal. *Weld. Met. Fabr.* **1969**, *37*, 327–339.
6. Chai, C.S.; Eagar, T.W. Slag metal reactions in binary CaF_2-metal oxide welding fluxes. *Weld. J.* **1982**, *61*, 229–232.
7. Dallam, C.B.; Liu, S.; Olson, D.L. Flux composition dependence of microstructure and toughness of submerged arc HSLA weldments. *Weld. J.* **1985**, *64*, 140–152.
8. Palm, J.H. How fluxes determine the metallurgical properties of Submerged Arc Welds. *Weld. J.* **1972**, *51*, 358–360.
9. Paniagua-Mercado, A.M.; Lopez-Hirata, V.M.; Saucedo Munoz, M.L. Influence of the chemical composition of flux on the microstructure and tensile properties of submerged-arc welds. *J. Mater. Process. Technol.* **2005**, *169*, 346–351. [CrossRef]
10. Bang, K.; Park, C.; Jung, H.; Lee, J. Effects of flux composition on the element transfer and mechanical properties of weld metal in submerged arc welding. *J. Met. Mater. Int.* **2009**, *15*, 471–477. [CrossRef]
11. Singh, B.; Khan, Z.A.; Siddiquee, A.N. Effect of flux composition on element transfer during Submerged Arc Welding (SAW): A literature review. *Int. J. Curr. Res.* **2013**, *5*, 4181–4186.
12. ESAB: Technical Handbook Submerged Arc Welding. 2021. Available online: https://assets.esab.com/asset-blank/assetfile/12295.pdf (accessed on 13 June 2021).
13. O'Brien, A. *Welding Handbook; Part 1*, 9th ed.; American Welding Society (AWS): Miami, FL, USA, 2004.
14. Hallén, H.; Johansson, K.-E. Use of a Metal Powder for Surface Coating by Submerged Arc Welding. U.S. Patent 6331688 B1, 18 December 2001.
15. Bong, W.L. System and Method for Metal Powder Welding. U.S. Patent 8946582 B1, 3 February 2015.
16. Patel, D.; Soman, S.N. Develop a flux cored wire for submerged arc welding of Ni-Mo low alloy steel. *Sadhana* **2020**, *45*, 127. [CrossRef]
17. Mitra, U.; Eagar, T.W. Slag metal reactions during submerged arc welding of alloy steels. *Metall. Trans. B* **1984**, *15*, 217–227. [CrossRef]
18. Burck, P.A.; Indacochea, J.E.; Olson, D.L. Effects of welding flux additions on 4340 steel weld metal composition. *Weld. J.* **1990**, *69*, 115–122.
19. Raabe, D.; Tasan, C.C.; Springer, H.; Bausch, M. From high-entropy alloys to high-entropy steels. *Steel Res. Int.* **2015**, *86*, 1127–1138. [CrossRef]
20. Moon, J.; Ha, H.-Y.; Kim, K.-W.; Park, S.-J.; Lee, T.-H.; Kim, S.-D.; Jang, J.H.; Jo, H.-H.; Hong, H.-U.; Lee, B.H.; et al. A new class of lightweight, stainless steels with ultra-high strength and large ductility. *Sci. Rep.* **2020**, *10*, 12140. [CrossRef]
21. Nand, S.; Singh, P.K. Effect of addition of metal powder on deposition rate, mechanical properties, and metallographic property of weld joints during Submerged Arc Welding process. *J. Mach. Form. Technol.* **2015**, *6*, 159–168.
22. Tušek, J.; Suban, M. High-productivity multiple-wire Submerged-Arc Welding and cladding with metal-powder addition. *J. Mater. Process. Technol.* **2003**, *133*, 207–213. [CrossRef]
23. Coetsee, T. Phase chemistry of Submerged Arc Welding (SAW) fluoride based slags. *Mater. Res. Technol.* **2020**, *9*, 9766–9776. [CrossRef]
24. Coetsee, T.; De Bruin, F.J. Improved titanium transfer in Submerged Arc Welding of carbon steel through aluminium addition. *Miner. Process. Extr. Metall. Rev.* **2021**, *43*, 771–774. [CrossRef]
25. Coetsee, T.; De Bruin, F.J. Reactions at the molten flux-weld pool interface in submerged arc welding. *High Temp. Mater. Processes.* **2021**, *40*, 421–427. [CrossRef]
26. Coetsee, T.; De Bruin, F. Application of Copper as Stabiliser in Aluminium Assisted Transfer of Titanium in Submerged Arc Welding of Carbon Steel. *Processes* **2021**, *9*, 1763. [CrossRef]
27. Coetsee, T.; De Bruin, F. Chemical Interaction of Cr-Al-Cu Metal Powders in Aluminum-Assisted Transfer of Chromium in Submerged Arc Welding of Carbon Steel. *Processes* **2022**, *10*, 296. [CrossRef]
28. Coetsee, T.; De Bruin, F. Aluminium-Assisted Alloying of Carbon Steel in Submerged Arc Welding: Application of Al-Cr-Ti-Cu Unconstrained Metal Powders. *Processes* **2022**, *10*, 452. [CrossRef]
29. Kluken, A.O.; Grong, Ø. Mechanisms of inclusion formation in Al-Ti-Si-Mn deoxidized steel weld metals. *Metall. Trans. B* **1989**, *20*, 1335–1349. [CrossRef]
30. Bale, B.R.; Bélisle, E.; Chartrand, P.; Degterov, S.A.; Errikson, G.; Hack, K.; Jung, I.-H.; Kang, Y.-B.; Melançon, J.; Pelton, A.D.; et al. FactSage thermochemical software and databases-recent developments. *Calphad* **2009**, *33*, 295–311. [CrossRef]
31. Polar, A.; Indacochea, J.E.; Blander, M. Electrochemically generated oxygen contamination in submerged arc welding. *Weld. J.* **1990**, *69*, 68–74.
32. Lau, T.; Weatherly, G.C.; Mc Lean, A. The sources of oxygen and nitrogen contamination in submerged arc welding using CaO-Al_2O_3 based fluxes. *Weld. J.* **1985**, *64*, 343–347.
33. Mitra, U.; Eagar, T.W. Slag-metal reactions during welding: Part II. Theory. *Metall. Trans. B* **1991**, *22*, 73–81. [CrossRef]
34. Gött, G.; Gericke, A.; Henkel, K.-M.; Uhrlandt, D. Optical and spectroscopic study of a submerged arc welding cavern. *Weld. J.* **2016**, *95*, 491–499.
35. Zhang, J.; Coetsee, T.; Basu, S.; Wang, C. Impact of gas formation on the transfer of Ti and O from TiO_2-bearing basic fluoride fluxes to submerged arc welded metals: A thermodynamic approach. *Calphad* **2020**, *71*, 102195. [CrossRef]

36. Coetsee, T.; Mostert, R.J.; Pistorius, P.G.H.; Pistorius, P.C. The effect of flux chemistry on element transfer in Submerged Arc Welding: Application of thermochemical modelling. *Mater. Res. Technol.* **2021**, *11*, 2021–2036. [CrossRef]
37. Zhang, J.; Coetsee, T.; Wang, C. Element transfer behaviors of fused CaF_2-SiO_2 fluxes subject to high heat input submerged arc welding. *Metall. Trans. B* **2020**, *51*, 16–21. [CrossRef]
38. Zhang, J.; Coetsee, T.; Dong, H.; Wang, C. Element transfer behaviors of fused CaF_2-SiO_2-MnO fluxes under high heat input submerged arc welding. *Metall. Trans. B* **2020**, *51*, 885–890. [CrossRef]
39. Zhang, J.; Coetsee, T.; Dong, H.; Wang, C. Element Transfer Behaviors of fused CaF_2-TiO_2 Fluxes in EH36 Shipbuilding steel during high heat input Submerged Arc Welding. *Metall. Trans. B* **2020**, *51*, 1953–1957. [CrossRef]